Structural Behaviour of Prefabricated Composite Cold-Formed Steel and Timber Flooring Systems

Dheeraj Karki[1]; Harry Far[2]; Shami Nejadi[3]

[1]Corresponding author: PhD student in School of Civil and Environmental Engineering, Faculty of Engineering and Information Technology, University of Technology Sydney (UTS), Building 11, Level 11, Broadway, Ultimo, NSW 2007 (PO Box 123), Email: Dheeraj.karki@student.uts.edu.au

[2]Senior Lecturer of Structural Engineering, Faculty of Engineering and Information Technology, University of Technology Sydney (UTS), Building 11, Level 11, Broadway, Ultimo, NSW 2007 (PO Box 123), Email: Harry.Far@uts.edu.au

[3]Associate Professor of Structural Engineering, Faculty of Engineering and Information Technology, University of Technology Sydney (UTS), Building 11, Level 11, Broadway, Ultimo, NSW 2007 (PO Box 123), Email: Shami.Nejadi@uts.edu.au

Abstract:

In this study, structural performance of a new type of lightweight composite cold-formed steel and timber (CFST) flooring system has been investigated by conducting four-point bending tests on thirteen specimens. A bare cold-formed steel system without timber sheathing was also tested to provide a benchmark response to which the strength and stiffness of the composite system were compared. This paper presents key findings on the flooring system's structural behaviour and performance parameters, such as ultimate bending capacity, load-deflection response, load-slip response and failure modes, by categorising thirteen specimens into four sub-groups based on shear connector types and spacings. In the proposed composite CFST flooring system, 45mm thick

structural plywood panels were connected to the 2.4mm thick cold-formed steel C-section joist using self-drilling screws, coach screws, and nuts and bolts. The performance of different types of shear connectors on the composite action is experimentally investigated and compared with the theoretical plastic section. Furthermore, the load-carrying capacity, effective bending stiffness, and deflection of composite CFST beams were computed theoreticall using elastic theory and compared to experimental results, which showed good agreement.

Keywords*: Cold-formed steel joists; Structural plywood; Composite floors; Four-point bending tests; Shear connection; Composite action; Flexural behaviour; Modular buildings; Composte beams*

1 INTRODUCTION

For the development of lightweight flooring systems, cold-formed steel (CFS) joists or beams can be suitable structural members over timber joists due to their high strength-to-weight ratio, fast installation, and good resistance to fire and termite [1-3]. The use of engineered timber floorboard sheathing along with CFS joists provides lateral restraint to the CFS joists and the use of sustainable materials like steel and timber will also contribute to the eco-friendly floors making it an economical and durable solution for residential floors [4, 5]. CFS joists and engineered timber floorboard can be connected by various mechanical fasteners, which act as shear connectors to provide a composite action phenomenon [4, 6, 7].

The most widespread use of composite structures is in the construction of floors and slabs. When a floor assembly is loaded, the load is transferred from the sheathing through the shear connectors to the floor joist, forming a composite assembly in which the load is distributed between two materials providing superior strength and stiffness over individual members themselves [8]. There have been numerous research works on composite steel-concrete and timber-concrete floors performed in the past, and many investigations have been carried out for development of shear connections. In

comparison, the benefit of composite construction, e.g., hot-rolled steel and concrete [9, 10], timber and concrete [11, 12], and hot-rolled steel and timber [13, 14] are well established and understood with a few recent studies on lightweight floors with CFS joists and timber [6, 15-18]. The use of CFS and timber floorboard contributes to the lightweight floor making it vulnerable to certain vibration problems due to their reduced mass and lower structural damping. Experimental investigations to study the dynamic performance of these floors [19, 20] has identified various construction details to control annoying vibrations without considering the mobilisation of composite action due to the presence of shear connection. Studies [21-23] have presented design procedures to check the acceptability of floors for vibration serviceability but there are limited studies that consider the contribution of shear connection on the structural capacity of these floors leading to conservative designs of CFS joists.

Karki and Far [24] have discussed the state of the art on composite cold-formed steel floors. Experimental and numerical investigations conducted by Zhou et al. [6] and Kyvelou et al. [15, 25] have demonstrated enhancement in the load-carrying capacity and stiffness of the composite CFS and timber-based flooring systems due to the consideration of composite action arising due to self-drilling screws (SDS) as shear connectors. Further parametric studies conducted by Karki et al. [26] on composite cold-formed steel flooring systems highlighted the importance of shear interaction that arose at the top flange of the CFS joist and the bottom surface of timber floorboard and demonstrated the high strength-to-weight ratio of the flooring system. It has become apparent from the existing literature that only SDS was used as shear connectors in cold-formed steel and timber-based flooring systems. Hence to overcome the current knowledge gaps, there is a need to investigate the performance of different types of mechanical fasteners with higher ductility as shear connectors to be used in this type of flooring system.

The purpose of this study is to discuss a novel composite cold-formed steel and timber (CFST) floor module that comprises a CFS C-section joist and structural plywood panel as floor sheathing. Four different types of shear connectors are used to fabricate the modular floor components by combining CFS C-section and structural plywood panels. The main advantage of these modular floor components is that they can be fabricated off-site and easily and quickly assembled on-site, which reduces the construction time that will effectively address the current housing demand. CFST flooring systems offer the advantage of a high strength-to-weight ratio and lead to less seismic and gravity load on the foundation of the buildings. CFST floor module can be easily and quickly fixed to the main structural steel beams using only bolts or screws with cleat brackets at the end of the joists. The use of timber panels along with the steel joist reflects the growing awareness of environmental issues in new construction making it a sustainable choice [27, 28]. A typical reference construction system and assembly method of the CFST prefabricated floor components is shown in Fig. 1. In this paper, the flexural behaviour of the composite CFS C-section and structural plywood flooring system is experimentally and analytically investigated. As part of an experimental study, four-point bending tests were conducted on thirteen composite beam specimens and one bare CFS system (used as a benchmark study for comparative purposes). The bending capacity and flexural stiffness of the considered composite CFST beams were theoretically calculated based on the plastic analysis approach to summarise the findings of the four-point bending tests. An analytical model is also proposed for calculation of ultimate elastic load-carrying capacity and mid-span deflection of the composite CFST beams, which can be used for practical applications.

2 EXPERIMENTAL INVESTIGATION

2.1 Specimen Details

Thirteen 4-point bending tests were conducted on composite CFS and structural plywood flooring systems. A summary of tested composite systems with different means of shear connections is presented in Table 1. 254mm deep and 2.4mm thick CFS C-sections were employed as floor joists with 45mm thick F17 grade structural plywood panels as sheathing. Material tests of CFS C-section and plywood panels were conducted as per AS 1391:2007 [29], and AS/NZS 2269.1:2012 [30], respectively and the detail description of the tests can be found in Karki et al. [31]. The average measured mechanical properties of the CFS joist and plywood panel is provided in Tables 2 and 3, respectively. A bare CFS system was also tested to provide a benchmark response for which the remaining composite systems could be compared. For all the specimens, adhesives were applied at the joints between adjacent plywood panels.

2.2 Test setup and procedure

The overall test layout for all beam tests is shown in Fig. 2. All the tested composite beams consist of two CFS joists, back to back faced 600mm apart, and were connected to plywood floor sheathing with different means of shear connection and various spacings. For the bare CFS system, 50x50x3 mm equal steel angles were used to restrain the top flanges of the two joists, as depicted in Fig. 3. The beams were supported simply on pin and roller across a 4.5m span with 100mm overhang from each support. A spreader beam was used to transfer the load from the loading jack through load-bearing spherical to two loading beams running across the width of the plywood. The spherical bearings have a concave spherical surface in the housing washer that matches a convex surface on the shaft washer. They can primarily withstand axial loads and also combined axial and radial loads,

therefore no axial force would be applied to the beam. Longitudinal slips at the ends of the beams were measured using four LVDTs at each end, whereas the vertical deflection at the midspan of the beam was recorded using string potentiometers beneath each CFS joist. Strain gauges were fixed along the height and width of the midspan cross-section to take the readings of strain distribution during the testing and, ultimately, to locate the position of neutral axes through the depth of composite sections. Fig. 4 and 5 illustrate the employed instrumentation for all the bending tests. The CFS joist's webs were stiffened locally at supports and loading points using 12mm thick (Grade 350) steel plates on either side, held in place by M16 (Grade 8.8) through rods. This was done to avoid the localised failure of the CFS web and to assist in equal distribution of loading by preventing any possible twisting.

The load was applied using a single hydraulic actuator (MTS 201.35) connected in a closed loop PID control system (MTS FlexTest 60), utilising a customisable portal load frame and concrete support blocks. The single actuator utilised suitably stiff spreader beams with suitable connections to apply two line loads across the deck at $1/3^{rd}$ and $2/3^{rd}$ spans of equal loads. Data were acquired utilising a NI PXIe-1083 chassis with PXIe-4330 modules and a single PXIe-4302 module. Flexlogger was used for acquiring the test data at a rate of 100Hz. All sensors were internally calibrated before testing. All the tests were carried out in displacement control condition and statically loaded to obtain the ultimate bending load. Each specimen was loaded up to 10% of the estimated ultimate load to ensure the correct functioning of the instrumentation and settling of the specimen. Afterwards, the load was gradually applied up to failure at a displacement rate of 1mm/min.

2.3 **Test results**

A total of thirteen prefabricated composite cold-formed steel and plywood flooring system with dimensions 1.2m x 4.5m were tested in bending to investigate the flexural strength and stiffness as a

result of composite action that arises between the interface of CFS joist and plywood due to the use of various fasteners. Two distinctive failure characteristics were observed in the tests. The specimens with 400mm and 800mm fastener spacing exhibited distortional buckling of the top flange of the CFS joist between the fixings in the constant moment region, as shown in Fig. 6. While the specimens with 200mm spacing (namely SP-3, SP-6, and SP-10) exhibited bending due to the rotation in the bottom flange of CFS joist near the supports. This failure mode is depicted in Fig. 7. Similarly, the failure mode of the bare CFS system is illustrated in Fig. 8. Local buckling was observed on the top flange of the CFS section with approximate half wavelength of 150mm.

It is obvious that the composite specimens with 200mm fastener spacing are stronger and stiffer than their 400mm spacing counterparts; hence the specimens with 200 mm spacing demonstrated the tensile yielding of the bottom flange near the supports, concluding that yield strength of the CFS joist governed the ultimate capacity of SP-3, SP-6, and SP-10. It was observed in almost all the specimens that reducing the fastener spacing, the position of the neutral axis moved toward the top of the section as a result of increasing degree of shear connection. During the test, strain gauges were used to measure the strain profile along the cross-section at mid-span which comprised the area of the composite floor marked by the maximum bending moment and absence of shear force. The cross-section strain distribution at the ultimate load (P_u) and 50% of the ultimate load (0.5 P_u) through the depth of all specimens are illustrated and discussed. A linear response could be observed for all the specimens up to failure. All the specimens exhibited comparable behaviour characterised by compression and tension on plywood sheathing and tension in CFS joist. The key results of the specimens with different shear connectors are tabulated in Table 4, in which M_u is the moment capacity, δ_u is the average vertical midspan deflection at ultimate load, S_u is the average slips at the ends of the beam at ultimate load, and EI is the flexural stiffness of the composite beam.

2.3.1 *Connection with self-drilling screws*

Fig. 9 depicts the load-deflection responses of the specimens with 6mm diameter self-drilling screws. SDS at 400 mm centres and glue at the interface exhibited 10% higher moment capacity and flexural stiffness than SDS at 400 mm centres only. However, SDS at 200 mm centres has a 20% higher moment capacity than 400 mm centre screws. The cross-section strain distribution at the ultimate load and 50% of the ultimate load through the depth of specimens SP-3 and SP-4 at the mid-span is illustrated in Fig. 10.

2.3.2 *Connection with coach screws*

The load-deflection curves of the composite beam specimens with 12mm diameter coach screws are shown in Fig. 11. As can be seen, four specimens with different spacings and arrangements were tested. Failure of all specimens ultimately was governed by the yield strength of the CFS joist. Connections with coach screws at 400 mm centres with and without glue have similar loading capacities. The specimen with glue at the interface demonstrated 15% higher stiffness up to serviceability load, and after that, the stiffness of both specimens was similar. The sudden drop in the load-deflection response of the glued sample is because of the brittle failure of the adhesive bond on each joist and plywood interface, and afterwards, the coach screw started to take the flexural load. The specimen with coach screw at 200mm centres showed only 4% higher moment capacity but 15% higher flexural stiffness than the specimen with coach screw at 400 mm spacing. The distribution of strain through the depth of specimens at the mid-span is shown in Fig. 12.

2.3.3 *Connection with M8 nut and bolt*

The load-deflection responses of the composite beam specimens with M8 nut and bolt are shown in Fig. 13. The specimen with 200 mm spacing demonstrated minimal enhancement in the ultimate strength and stiffness, which is only 6 % and 5 % higher than 400 mm spacing. It can be observed

that with an increasing degree of shear connection, the neutral axis position in the CFS joist moved toward the top of the section, as can be seen in Fig. 14.

2.3.4 *Connection with M12 nuts and bolts*

Four specimens with different shear connection arrangements were tested, and the load-deflection histories and cross section strain distribution of all the tested specimens are presented in Fig. 15 and 16 respectively. From the push-out tests as presented by Karki et al. [31], it was understood that M12 nuts and bolts provide the most ductile and stiffest shear connections compared to other fasteners; hence 400 mm and 800mm fastener spacing was chosen for this composite floor assembly. 400 mm nuts and bolts spacing achieves 20% higher moment capacity and 11% higher stiffness than 800 mm spacing. The influence of structural adhesives for the 800 mm spacing on the stiffness was only 5%, but the strength capacity was enhanced by 10%.

2.4 **Summary of experimental findings**

One of the main purposes of this study was to experimentally investigate the shear connector's performance of different fastener types on the structural behaviour of composite cold-formed steel and timber flooring systems. Hence in this section, more comparative findings are discussed. In Fig. 17, the load-deflection histories of composite specimens that utilise self-drilling screws, M12 coach screws, M8 nuts and bolts, and M12 nuts and bolts as shear connectors at 400 mm spacings are compared with bare CFS beam. The moment capacity was increased by 7%, 60%, 56%, and 58% for the composite specimens with SDS, M12-CS, M8-NB, and M12-NB, respectively, in comparison to the bare CFS joist alone. Figs. 17 and 18 display the maximum moment capacity and flexural stiffness of each specimen, nomralised by the moment capacity, M, and flexural stiffness, EI, of the corresponding CFS beam. As expected, all the tested specimens exhibited composite action phenomenon and hence improvement in the strength and stiffness capacities. As can be seen from the

bar charts in Fig. 18 and Fig. 19, the spacing of the fasteners and the application of structural adhesives at the CFS joist and plywood interface were found to have improved performance in the moment capacity and flexural stiffness of these lightweight flooring systems. It was also observed that the presence of unstiffened web holes does not have noticeable influence on the structural performance of these flooring systems.

For ductile connections like the M12 coach screws and M12 nuts and bolts at 400mm spacing, the moment capacity was significantly enhanced (by more than 50%), and flexural stiffness was improved by 19% and 22% only. However, for the M12 coach screw at 200 mm spacing, the flexural stiffness was found to be increased by 40%, but the moment capacity was similar to that of 400 mm spacing. Hence from this observation, it has become clear that there is a trade-off between the ductility and spacing of shear connectors with the yield strength of the CFS joist in these flooring systems.

3 PLASTIC ANALYSIS OF RESULTS

Inorder to achieve the full shear connection, the number of fasteners provided should be enough so that the full plastic bending capacity can be achieved with maximum use of material strength[32, 33].

3.1 Theoretical plastic bending resistance and flexural stiffness assuming full shear interaction

The theoretical plastic bending resistance of the composite section can be determined considering full composite action between the plywood panel and CFS joist with the plastic distribution of stresses. Two possible scenarios are considered; Fig. 19 illustrates the case where the plastic neutral axis (PNA) lies within the plywood panel, and Fig. 20 illustrates the case where PNA lies within the steel section. Assuming a full shear connection for the tested composite system, the plastic compressive force in the plywood sheathing was calculated to be N_p = 756 kN. Since the compressive force of

plywood (756 kN) is greater than the tensile force in steel beam (A_{st} x F_y = 550 kN), hence theoretical plastic neutral axis lies in the plywood sheathing.

For the scenario shown in Fig. 19, the force equilibrium can be expressed as:

$$N_S + N_{p,t} = N_{p,c} \tag{1}$$

$$A_S F_y + A_{pt} F_{tp} = A_{pc} F_{cp} = b_{eff} t_a F_{cp} \tag{2}$$

Where A_s is the area of the CFS section, F_y is the yield strength of CFS, F_{tp} and $F_{cp}$are the tensile and compressive strength of the plywood, respectively, b_{eff} is the effective width of plywood sheathing (taken as 600 mm). The plastic moment capacity of the composite section (about the axis of the compressive force $N_{p,c}$) can be calculated as:

$$M_{pl} = N_s Z + N_{p,t} \frac{t_p}{2} \tag{3}$$

In which $$Z = h - t_a/2 - y_c \tag{4}$$

Where h is the height of the composite section, and y_c is the distance from the bottom flange to the centroid of the steel section. The plastic moment capacity of the tested composite system was calculated as M_{pl}= 81.46 kN.m using the force equilibrium expression as shown in Fig. 19 and Equations (1) to (4).

The stiffness of the composite system is determined by transforming the area of plywood sheathing into an equivalent area of steel, as demonstrated in Fig. 21.

$$I_{comp} = I_s + \frac{b_{eff} t_p^3}{12n} + A_s (y_{el} - y_c)^2 + \frac{A_p}{n}\left(y_{el} - h - \frac{t_p}{2}\right)^2 \tag{5}$$

Where, I_s and A_s are the second moment of area and area of the steel section, A_p is the area of plywood, and n is the ratio of elastic moduli of steel to plywood. y_{el} is the distance from the bottom flange of the steel to the centroid of the composite section and is determined from Equation (6).

$$y_{el} = \frac{y_c A_s + \frac{A_p}{n}\left(h_s + \frac{t_p}{2}\right)}{A_s + \frac{A_p}{n}} \tag{6}$$

For the composite beam examined in this study, using Equations (5) and (6), the second moment of area I_{comp} is determined to be 22.9x10^6 mm^4.

3.2 **Comparison of experimental results with full composite plastic bending capacity and flexural stiffness**

The ultimate moment capacity $M_{u,exp}$ and flexural stiffness $(EI)_{exp}$ of each of the examined composite beams normalised by theoretical moment capacity $M_{pl,r}$ and flexural stiffness $(EI)_{comp}$ of the fully composite system are presented in Fig. 22 and 23, respectively. As expected, the system with self-drilling screws exhibited lesser capacity than others. The more ductile and at closer spacing the shear connection between the CFS joist and plywood sheathing, the closer the moment capacities and flexural stiffness were to those of equivalent fully composite system.The specimen with superior ductile connections like the M12 coach screw and M12 nuts and bolts demonstrated higher strength and stiffness than the others by attaining around 80% of the plastic moment capacity and 70% of the flexural stiffness of the fully composite system. It is worth noting that the system with M8 nuts and bolts at 400mm spacing demonstrated substantial moment capacity than that of M12 nuts and bolts at 800mm spacing which demonstrated the fact that shear connection spacing at denser spacing perform best. Similarly the specimens with SDS at 200mm spacing exhibited similar capcities than that of

specimens with M12 nuts and bolts at 800mm spacing which also demonstrated the importance of ductility of shear connectors for this type of flooring system.

4 ELASTIC ANALYSIS OF RESULTS

It is nearly impossible for the composite cross-section to act monolithically without slip at the beam-board interface (full shear interaction) because all fasteners will deform with increasing load. [9, 34]. Since slip develops at the interface, and the failure of the shear connection or material yielding affects load-carrying capacity in all the tested composite systems; the shear interaction are assumed to be partial. Therefore the elastic moment resistance of the composite system with the partial shear connection varies between the elastic moment capacity of the bare CFS beam and the elastic moment capacity of the fully composite beam. Note that cold-formed steel sections are thin-walled, and their section moment capacity is limited due to their susceptibility to local instabilities like distortional or local buckling [35, 36]; hence calculation is done in accordance with the direct strength method (DSM) of AS/NZS 4600:2018 [37]. THIN WALL-2 [38] is used in this study to develop the signature curve of the buckling stress versus buckling half-wavelength for the C-section. THIN-WALL is a finite strip software employed to extract the pure local and distortional buckling mode shapes by performing elastic buckling analysis. Fig. 24 and 25 depicted the signature curve of the buckling load factor versus buckling half wavelengths for local and distortional buckling, respectively obtained from THIN-WALL. In Figures 25 and 26, the critical load factor plotted on the Y-axis is relative to the load required to cause first yield of the C-section. The local and distortional buckling stress was found to be 509 MPa and 430 MPa, respectively. It should also be mentioned that in all the composite beam tests, the governing failure mode was the distortional buckling of top flange between the connections. The elastic buckling analysis also shows that distortional buckling stress being the predominant mode cause the CFS C-section joist to yield first. Table 5 provides a summary of the

four-point bending tests of the CFS C-section, which includes the ultimate peak loads (P_u) and the tested bending moments (M_t). The elastic local buckling moment (M_{ol}), elastic distortional buckling moment (M_{od}), the yield moment (M_y) based on tensile coupon test results, and plastic moment (M_p) are also presented in Table 5. M_{ol} and M_{od} are calculated by multiplying elastic section modulus (Z) with the local buckling stress (F_{ol}) and distortional buckling stress (F_{od}), respectively. As can be seen from the values summariseded in Table 5, the tested moment capacity of the C-section is slightly larger than the yielding moment or local buckling moment capacity, which is relatable to the inelastic reserve capacity of cold-formed thin-walled steel sections [39]. Hence, the yield strength of CFS is reasonable to be used for computation of elastic ultimate bending moment of CFST beams.

4.1 **Theoretical elastic bending capacity of CFST beams**

Based on the research conducted by Hsu et al. [40] and Liu et al. [41] on the performance of CFS-concrete and steel timber composite beams, respectively, similar assumptions and methodology is adopted in this study to investigate the elastic bending capacity of composite CFST beams. Under serviceability load conditions, both the CFS and plywood panel are in elastic stage. To calculate the elastic bending capacity of CFST beams following assumptions are made:

- Under the flexure assumption, plywood sheathing and cold-formed steel joist that comply with the plane section remain plane;
- Both steel and timber are ideal linear elastic bodies;
- When the slip occurs at the interface, the curvature of plywood sheathing and cold-formed steel remains the same, and the lifting effect may be ignored.

If the plywood sheathing of CFST beams were damaged first, the elastic bending capacity M_{el} with the full shear connection could be calculated according to Equation (7). When the failure in CFST

beams is initiated by yielding cold-formed steel, M_e can be computed as per Equation (8). The ultimate elastic bending moment of the CFST beam with the full shear interaction may be taken as the smaller value of Equation (7) or (8).

$$M_{el} = f_{yp} I_T n / z \tag{7}$$

$$M_{el} = f_{ys} I_T / z \tag{8}$$

Where f_{yp} denotes parallel to grain compression strength of plywood panel (MPa), f_{ys} denotes the yield strength of cold-formed steel (MPa), I_T (mm^4) is the transformed section moment of inertia which is calculated as per Equation (10), n is the ratio of elastic moduli of steel to plywood (E_s/E_p), z is the centroidal position of transformed section (mm) and determined from Equation (9)

$$z = \frac{A_s Z_1 + A_t z_2 / n}{A_s + A_t / n} \tag{9}$$

Considering the slip between the CFS and plywood interface, the actual bending capacity of composite CFST beams with a partial shear connection can be calculated according to Equation (10).

$$M = M_{el} - \Delta M \tag{10}$$

Where, M_{el} is the elastic bending capacity of CFST beams with full shear interaction, ΔM is the moment due to slip strain. It is assumed that when the slip occurs at the interface, the curvature of plywood sheathing and cold-formed steel remains the same at a given section, and the lifting effect may be ignored. Hence, the additional curvature ($\Delta\Phi$) due to slip strain ($\varepsilon_{s'}$) of CFST beams with partial shear interaction can be calculated according to Equations (11) and (12). The strain distribution in composite CFST beams under elastic bending is represented in Fig. 26.

$$\Delta\Phi = \frac{\varepsilon_{s\prime t}}{h_t} = \frac{\varepsilon_{s\prime s}}{h_s} = \frac{\varepsilon_{s\prime t} + \varepsilon_{s\prime s}}{h_t + h_s} = \frac{\varepsilon_{s\prime}}{h} \tag{11}$$

$$\varepsilon_{s\prime} = h\Delta\Phi \tag{12}$$

Where $\varepsilon_{s\prime t}$ and $\varepsilon_{s\prime s}$ are the strains at the bottom of the plywood and top of cold-formed steel due to the stiffness of connections, $\varepsilon_{s\prime}$ denotes the slip strain at the CFS and plywood interface.

The strain at the top of CFS ($\varepsilon_{s\prime s}$) can be found by rearranging Equation (11)

$$\varepsilon_{s\prime s} = \frac{h_s}{h}\varepsilon_{s\prime} \tag{13}$$

The tensile force variation in the CFS section due to slip (ΔN_S) can be computed according to Equation (14).

$$\Delta N_S = \sigma A = \varepsilon_{s\prime s} E_s \left(A_{sf} + \frac{1}{2} A_{sw}\right) = \frac{E_s \varepsilon_{s\prime s} h_s A_s}{2h} \tag{14}$$

A_{sf} (mm^2) is the area of top flange, A_{sw} (mm^2) is the area of web. The force equilibrium equation can be obtained from Equation (15).

$$\Delta N_S = \Delta N_t \tag{15}$$

Where ΔN_t denotes the resultant compressive force of additional stress for the plywood section. The moment ΔM due to slip strain can be computed according to Equation (16).

$$\Delta M = \frac{h_s}{6} E_s \varepsilon_{s\prime} A_s = \frac{M_{el} h h_s A_s (E_s I_T - EI_{eff})}{6EI_{eff} I_T + h h_s E_s A_s I_T} \tag{16}$$

4.2 **Effective bending stiffness of CFST beams**

The importance of determining effective bending stiffness for constructing timber-concrete composite floors was underlined in previous studies [42, 43] and a similar methodology is employed in this study. Previous studies [8, 44] estimated the deformation of steel and timber beams using Gamma (γ) method and found the experimental results to be close to the theoretical values. Most recently, Kyvelou et al. [33] proposed an equivalent formula based on the $\gamma - \text{method}$ to calculate the effective bending stiffness of cold-formed steel and particleboard flooring system. Hence, the effective bending stiffness for CFST beams in this study is calculated based on Appendix B of Eurocode 5 [45]. The obtained slip modulus values discussed in Karki et al. [31] are used to calculate the effective bending stiffness of a cold-formed steel and timber composite assembly. Shear bond coefficient, γ, is calculated first to obtain the effective bending stiffness value of a composite assembly using Equation (17).

$$\gamma = \frac{1}{1 + \frac{\pi^2 S E_t A_t}{K L^2}} \tag{17}$$

In Equation (17), γ is shear bond coefficient, S is the spacing of shear connections (mm), E_t is the modulus of elasticity of timber floorboard (MPa), A_t is the area of timber floorboard (mm^2), K is the slip modulus (N/mm), and L is the length of the member (mm). The effective stiffness $(EI)_{eff}$ of the cold-formed steel and timber composite assembly can be determined using Equation (18).

$$(EI)_{eff} = E_t I_t + \gamma E_t A_t a1^2 + E_s I_s + E_s A_s a2^2 \tag{18}$$

Where I_t is the moment of inertia of timber floorboard, a1 is the distance between the centroid of timber and centroid of composite assembly, E_s is the modulus of elasticity of CFS, I_s is the moment of inertia of CFS, A_s is the area of CFS , a2 is the distance between the centroid of CFS and composite assembly. The distance between the CFS joist centroid and the centroid of the composite assembly can be determined from Equations (19) and (20).

$$a2 = \frac{\gamma E_t A_t (h_s + h_t)}{2(\gamma E_t A_t + E_s A_s)} \quad (19)$$

$$a1 = \frac{1}{2}(h_s + h_t) - a2 \quad (20)$$

The degree of composite action in the specimens can be quantified by the composite efficiency (η_{ef}) as shown in Equation (21) based on the effective bending stiffness using Gamma method.

$$\eta_{ef} = \frac{EI_{partial} - EI_{non\ composite}}{EI_{full\ composite} - EI_{non\ composite}} x100\% \quad (21)$$

Where $EI_{partial}$ denotes the effective bending stiffness of the composite specimens with partial shear connections (N.mm^2); $EI_{non\ composite}$ denotes the stiffness of a system without connections between the members (N.mm^2); $EI_{full\ composite}$ denotes the stiffness of a perfectly rigid composite system or full shear interaction (N.mm^2). The composite efficiency obtained from Equation (21) are given in Table 6 which also clearly demonstrates the higher composite efficiency of ductile shear connectors at closer spacings and glued connections too. The ratio of effective bending stiffness obtained from Gamma method to the experimental values is also presented in Table 6 which demonstrate the accuracy of Gamma method with the mean value of 1.02.

The mid-span deflection of a simply supported beam loaded at its third point with two equal concentrated loads P can be calculated using Equation (22) in accordance with the theory of elasticity.

$$\delta = 23PL^3/648EI_{eff} \quad (22)$$

4.3 **Comparison of experimental and theoretical elastic calculations**

Table 7 present the results of the comparison between the theoretical elastic bending moment values and mid-span deflection values obtained according to the proposed analytical methods discussed in sections 4.1 and 4.2 and the physical test values. In Table 7, $M_{u,exp}$ is the moment capacity obtained

from the experiments, M_{el} is the elastic bending moment with full-shear interaction calculated in accordance with Equation (8), and M is the actual bending moment capacity with partial shear interaction of the CFST beams obtained using Equation (10). Similarly, δ_{exp} is the deflection of the composite CFST beam obtained from the experiments, and $\delta_{analytical}$ is calculated using Equation (22) by taking into account the effective bending stiffness. As can be seen from Table 6, the results calculated by the elastic analysis approach based on the composite coefficient method were in good agreement with the test values. The tested bending capacities of the composite beam utilising ductile shear connectors (M8 and M12 nuts and bolts and M12 coach screws) were found to be 20 to 28% higher than the capacities proposed by the elastic design approach. This approach produced slightly conservative results in comparison to the plastic analysis method, but this approach is believed to produce a safer design of such flooring systems in actual construction in the lack of extensive experimental data. The effective bending stiffness values of the composite CFST beams obtained experimentally and using the γ method were close. Therefore, the calculated deflection of the composite beams in the elastic stage demonstrated good results with the test observations. Hence, the proposed analytical methods can reliably be used to calculate the ultimate elastic bending capacity and mid-span deflection of composite CFST beams.

5 CONCLUSIONS

The experimental results of 13 full-scale composite CFST beams using cold-formed steel C-section sheathed with structural plywood panels are presented. The purpose of this research project was to explore the feasibility of composite action using four types of shear connectors with cold-formed steel flooring systems and to quantify the benefits derived from composite action. In this study, it was found that there are significant improvements in the structural performance of cold-formed steel flooring systems by utilising the shear interaction between the steel section and timber-based floor

sheathing. The ductility of fasteners and their spacing were found to have a substantial impact on the moment capacity and flexural stiffness of these systems. Up to 40% increament in the flexural stiffness was observed in the composite system in comparison with the bare steel system. In comparison to the bare CFS joist alone, the moment capacity for the composite CFST systems with 400mm fastener spacing was found to be increased by 6%, 47%, 54%, and 58% with SDS, M8 nuts and bolts, M12 coach screws and M12 nuts and bolts, respectively. Similarly, for the composite CFST system with 200mm fastener spacing, the moment capacity was enhanced by 27%, 56% and 60% for SDS, M8 nuts and bolts, and M12 coach screws. For stiffer connections like nuts and bolts and coach screws, the influence of fastener spacing on the moment capacity and flexural stiffness was not of too much difference as, in such cases, the capacity was found to be governed by the material strength of CFS or timber sheathing in comparison with the ductility of shear connectors.

Two approaches of design, namely plastic analysis and elastic analysis methods, are thoroughly discussed to quantify the test results. The elastic analysis approach described in this paper, which is based on the calculation of achieved degree of partial composite action, is advised to be employed in prediction of moment capacity and deflection of composite CFST beams. The proposed design methodology discussed herein enables to design for the improved structural performance to be achieved in cold-formed steel and timber flooring systems by utilising the shear interaction to establish the practical design rules to be used by practicing engineers.

Modular and prefabricated construction systems are a potential substitute for the fast construction of multi-story residential buildings. The pursuit of a more sustainable built environment has recently prompted the construction industry to develop energy-efficient systems. Buildings should indeed substantially decrease the amount of energy consumed throughout their entire life cycle, as well as the associated emissions of CO_2 into the environment. This paper has highlighted that the use of innovative construction techniques can assist with sustainability goals and is a good potential way to build green buildings.

References

[1] Hancock, G. J., "Cold-formed steel structures," *Journal of Constructional Steel Research,* vol. 59, no. 4, pp. 473-487, 2003/04/01/ 2003.https://doi.org/10.1016/S0143-974X(02)00103-7

[2] Hancock, G., "Cold-formed steel structures: Research review 2013–2014," *Advances in Structural Engineering,* vol. 19, no. 3, pp. 393-408, 2016.10.1177/1369433216630145

[3] Nash, "General guide to steel- framed building," National Association of Steel-Framed Housing, Victoria2007.

[4] Kyvelou, P., Reynolds, T. P. S., Beckett, C. T. S., and Huang, Y., "Experimental investigation on composite panels of cold-formed steel and timber," *Engineering Structures,* vol. 247, p. 113186, 2021/11/15/ 2021.https://doi.org/10.1016/j.engstruct.2021.113186

[5] Lawson, R. M., Ogden, R. G., Pedreschi, R., and Popo-Ola, S. O., "Developments of Cold-Formed Steel Sections in Composite Applications for Residential Buildings," vol. 11, no. 6, pp. 651-660, 2008.10.1260/136943308787543603

[6] Zhou, X., Shi, Y., Xu, L., Yao, X., and Wang, W., "A simplified method to evaluate the flexural capacity of lightweight cold-formed steel floor system with oriented strand board subfloor," *Thin-Walled Structures,* vol. 134, pp. 40-51, 2019.10.1016/j.tws.2018.09.006

[7] Henriques, J., Rosa, N., Gervasio, H., Santos, P., and Da Silva, L. S., "Structural performance of light steel framing panels using screw connections subjected to lateral loading," *Thin-Walled Structures,* vol. 121, pp. 67-88, 2017/12/01/ 2017.https://doi.org/10.1016/j.tws.2017.09.024

[8] Loss, C. and Davison, B., "Innovative composite steel-timber floors with prefabricated modular components," *Engineering Structures,* vol. 132, pp. 695-713, 2017/02/01/ 2017.https://doi.org/10.1016/j.engstruct.2016.11.062

[9] Ellobody, E. and Young, B., "Performance of shear connection in composite beams with profiled steel sheeting," *Journal of Constructional Steel Research,* vol. 62, no. 7, pp. 682-694, 2006/07/01/ 2006.https://doi.org/10.1016/j.jcsr.2005.11.004

[10] Rackham, J. W., Couchman, G. H., and Hicks, S. J., "Composite slabs and beams using steel decking: Best practice for design and construction," in "MCRMA Technical paper No.13," Steel Construction Institute2009.

[11] Deam, B. L., Fragiacomo, M., and Buchanan, A. H., "Connections for composite concrete slab and LVL flooring systems," *Material and Structures,* journal article vol. 41, no. 3, pp. 495-507, April 01 2008.10.1617/s11527-007-9261-x

[12] Lukaszewska, E., Fragiacomo, M., and Johnsson, H., "Laboratory Tests and Numerical Analyses of Prefabricated Timber-Concrete Composite Floors," *Journal of structural engineering,* vol. 136, no. 1, pp. 46-55, 2010.doi:10.1061/(ASCE)ST.1943-541X.0000080

[13] Hassanieh, A., Valipour, H. R., and Bradford, M. A., "Experimental and numerical study of steel-timber composite (STC) beams," *Journal of Constructional Steel Research,* vol. 122, pp. 367-378, 2016.10.1016/j.jcsr.2016.04.005

[14] Hassanieh, A., Valipour, H. R., and Bradford, M. A., "Composite connections between CLT slab and steel beam: Experiments and empirical models," *Journal of Constructional Steel Research,* vol. 138, pp. 823-836, 2017/11/01/ 2017.https://doi.org/10.1016/j.jcsr.2017.09.002

[15] Kyvelou, P., Gardner, L., and Nethercot, D. A., "Testing and Analysis of Composite Cold-Formed Steel and Wood−Based Flooring Systems," *Journal of Structural Engineering,* vol. 143, no. 11, 2017.10.1061/(asce)st.1943-541x.0001885

[16] Far, H., "Flexural Behavior of Cold-Formed Steel-Timber Composite Flooring Systems," *Journal of structural engineering,* vol. 146, no. 5, p. 06020003, 2020.doi:10.1061/(ASCE)ST.1943-541X.0002600

[17] Karki, D., Far, H., and Al-Hunity, S., "Determination of Slip Modulus of Cold Formed Steel Composite Members Sheathed with Plywood Structural Panels," *Steel and Composite Structures: an international journal,* vol. 43, pp. 511-522, 2022/05/26 2022.https://doi.org/10.12989/scs.2022.43.4.511

[18] Li, Y., Shen, H., Shan, W., and Han, T., "Flexural behavior of lightweight bamboo–steel composite slabs," *Thin-Walled Structures,* vol. 53, pp. 83-90, 2012/04/01/ 2012.https://doi.org/10.1016/j.tws.2012.01.001

[19] Xu, L. and Tangorra, F. M., "Experimental investigation of lightweight residential floors supported by cold-formed steel C-shape joists," *Journal of Constructional Steel Research,* vol. 63, no. 3, pp. 422-435, 2007.10.1016/j.jcsr.2006.05.010

[20] Parnell, R., Davies, B. W., and Xu, L., "Vibration Performance of Lightweight Cold-Formed Steel Floors," *Journal of structural engineering,* vol. 136, pp. 645-653, 2010.10.1061/(ASCE)ST.1943-541X.0000168

[21] Kraus, C. A. and Murray, T. M., "Floor Vibration design criterion for cold formed C shaped supported residential floor systems," Master of Science, Virginia polytechnic institute and state university, 1997.

[22] Zhang, S., "Vibration Serviceability of Cold-Formed Steel Floor Systems," Doctor of Philosophy Doctor of Philosophy, University of Waterloo, Waterloo, Ontario, Canada, 2017.

[23] Guan, Y., Zhou, X., Yao, X., and Shi, Y., "Vibration of cold-formed steel floors with a steel form deck and gypsum-based self-leveling underlayment," vol. 22, no. 13, pp. 2741-2754, 2019.10.1177/1369433219849836

[24] Karki, D. and Far, H., "State of the art on composite cold-formed steel flooring systems," *Steel Construction,* 2021.https://doi.org/10.1002/stco.202000026

[25] Kyvelou, P., Gardner, L., and Nethercot, D. A., "Finite element modelling of composite cold-formed steel flooring systems," *Engineering Structures,* vol. 158, pp. 28-42, 2018.10.1016/j.engstruct.2017.12.024

[26] Karki, D., Far, H., and Saleh, A., "Numerical Studies into Factors Affecting Structural Behaviour of Composite Cold-Formed Steel and Timber Flooring Systems," *Journal of Building Engineering,* p. 102692, 2021/05/09/ 2021.https://doi.org/10.1016/j.jobe.2021.102692

[27] Pasca, D. P., Aloisio, A., Fragiacomo, M., and Tomasi, R., "Dynamic Characterization of Timber Floor Subassemblies: Sensitivity Analysis and Modeling Issues," vol. 147, no. 12, p. 05021008, 2021.doi:10.1061/(ASCE)ST.1943-541X.0003179

[28] Ferrara, G., Michel, L., and Ferrier, E., "Flexural behaviour of timber-concrete composite floor systems linearly supported at two edges," *Engineering Structures,* vol. 281, p. 115782, 2023/04/15/ 2023.https://doi.org/10.1016/j.engstruct.2023.115782
[29] Standard Australia, *AS 1391-2007 Metallic materials -Tensile testing at ambient temperature*, SAI Global, 2007.
[30] Standard Australia, *AS/NZS 2269.1:2012 Plywood-Structural, Part 1: Determination of structural properties-Test methods*, SAI Global, 2012.
[31] Karki, D., Al-Hunaity, S., Far, H., and Saleh, A., "Composite connections between CFS beams and plywood panels for flooring systems: Testing and analysis," *Structures,* vol. 40, pp. 771-785, 2022/06/01/ 2022.https://doi.org/10.1016/j.istruc.2022.04.064
[32] Couchman, G. H., "Minimum degree of shear connection rules for UK construction to Eurocode 4," Steel Construction Institute2016.
[33] Kyvelou, P., Gardner, L., and Nethercot, D. A., "Design of Composite Cold-Formed Steel Flooring Systems," *Structures,* vol. 12, pp. 242-252, 2017.10.1016/j.istruc.2017.09.006
[34] Nie, J. and Cai, C. S., "Steel-Concrete Composite Beams Considering Shear Slip Effects," vol. 129, no. 4, pp. 495-506, 2003.doi:10.1061/(ASCE)0733-9445(2003)129:4(495)
[35] Hancock, G. J., *Design of Cold-formed Steel Structures: To Australian/New Zealand Standard AS/NZS 4600: 1996*. Australian Institute of Steel Construction, 1998.
[36] Yu, C. and Schafer, B. W., "Local Buckling Tests on Cold-Formed Steel Beams," *Journal of structural engineering,* vol. 129, no. 12, pp. 1596-1606, 2003.doi:10.1061/(ASCE)0733-9445(2003)129:12(1596)
[37] Standard Australia, *AS/NZS: 4600-2018 Cold-formed steel structures*, SAI Global, 2018.
[38] Case, "THIN WALL 2, A Computer Program for Cross-section Analysis and Finite Strip Buckling Analysis and Direct Strength Design of Thin-walled Structures," ed. Centre for Advanced Structural Engineering, School of Civil Engineering, The University of Sydney, 2006.
[39] Pham, C. H. and Hancock, G. J., "Experimental Investigation and Direct Strength Design of High-Strength, Complex C-Sections in Pure Bending," vol. 139, no. 11, pp. 1842-1852, 2013.doi:10.1061/(ASCE)ST.1943-541X.0000736
[40] Hsu, C.-T. T., Punurai, S., Punurai, W., and Majdi, Y., "New composite beams having cold-formed steel joists and concrete slab," *Engineering Structures,* vol. 71, pp. 187-200, 2014/07/15/ 2014.https://doi.org/10.1016/j.engstruct.2014.04.011
[41] Liu, J., Liu, R., Li, W., Wang, J., and Chen, L., "Experimental Study on the Flexural Performance of Timber–Steel Composite (TSC) I-Beams," vol. 12, no. 8, p. 1206, 2022.
[42] Ceccotti, A., "Composite concrete-timber structures," *Progress in Structural Engineering and Materials,* vol. 4, no. 3, pp. 264-275, 2002.
[43] Steinberg, E., Selle, R., and Faust, T., "Connectors for Timber-Lightweight Concrete Composite Structures," *Journal of structural engineering,* vol. 129, no. 11, pp. 1538-1545, 2003.doi:10.1061/(ASCE)0733-9445(2003)129:11(1538)

[44] Yang, R., Li, H., Lorenzo, R., Sun, Y., and Ashraf, M., "Flexural behaviour of steel timber composite (STC) beams," *Steel and Composite Structures,* vol. 41, no. 2, pp. 193-207, 2021.https://doi.org/10.12989/scs.2021.41.2.193

[45] Cen*, EN 1995-1-1:2004 Eurocode 5: Design of timber structures-Part 1-1: General-Common rules and rules for buildings*, European Committee for Standardization, 2004.

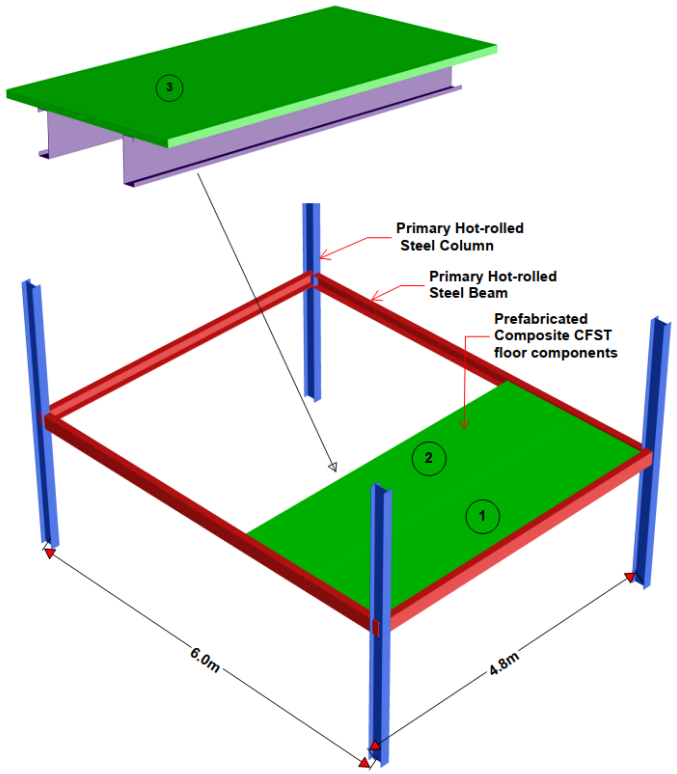

Fig. 1. Typical reference construction system and sequence of assembly for prefabricated composite floor components

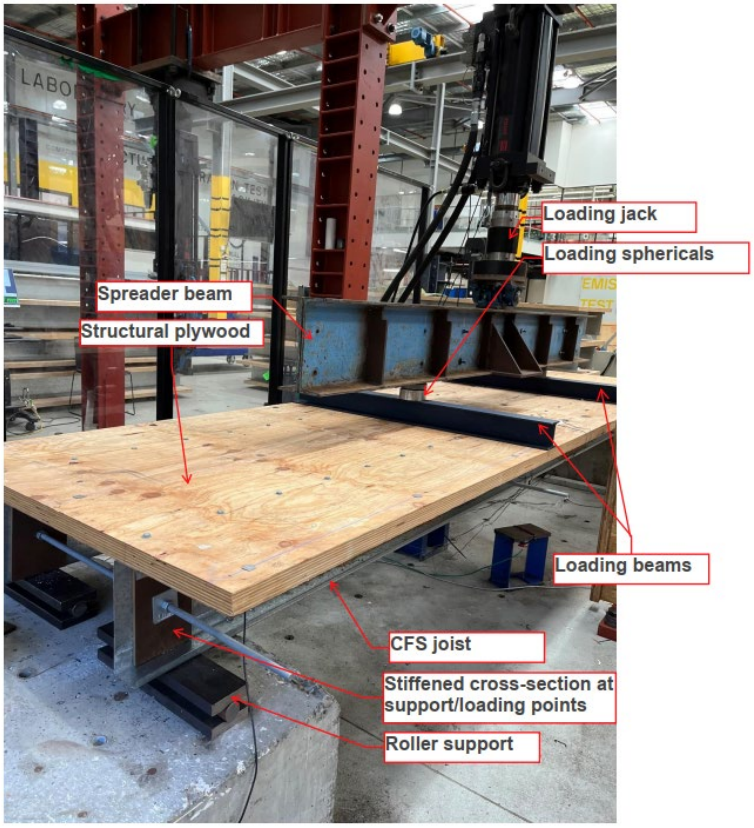

Fig. 2. Four-point bending test layout of composite beam tests

Fig. 3. Overall test layout of bare CFS beam tests

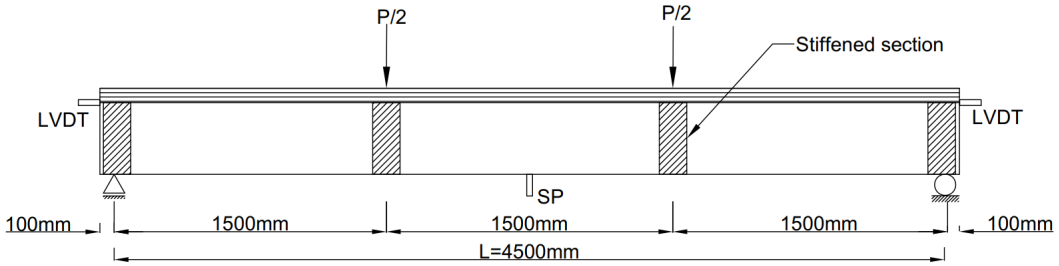

Fig. 4. Arrangement of instrumentation for composite beam tests

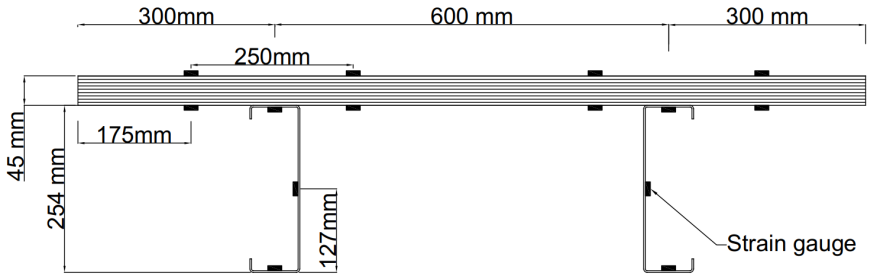
300mm
600 mm
300 mm
250mm
45 mm
175mm
254 mm
127mm
Strain gauge

Fig. 5. Strain gauges position at the mid span of cross section

Fig. 6. Distortional buckling between fixings in the constant moment span (Specimen SP-11)

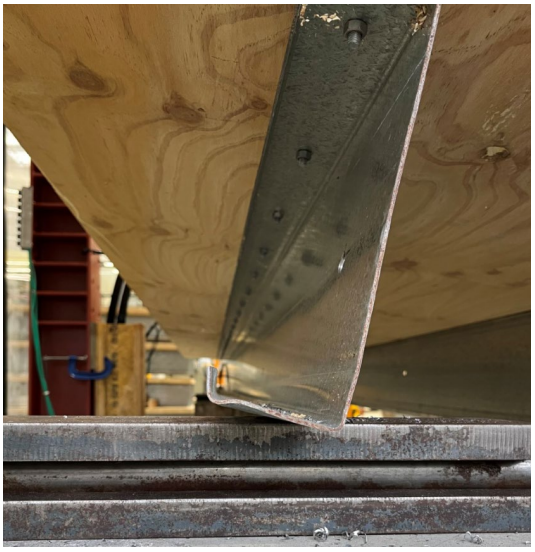

Fig. 7. Bottom flange rotation and bending near the supports (Specimen SP-10)

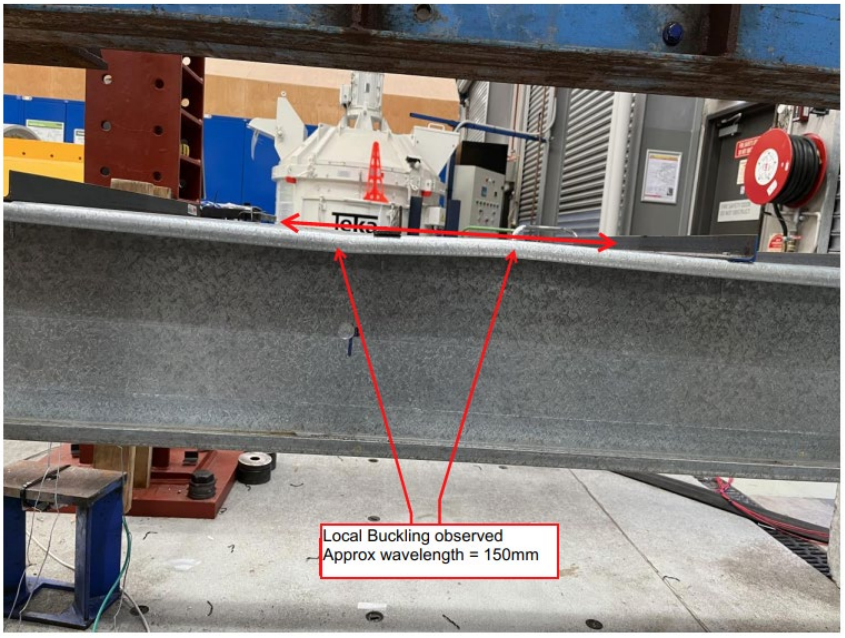

Fig. 8. Local buckling observed between angle restraints for bare CFS system

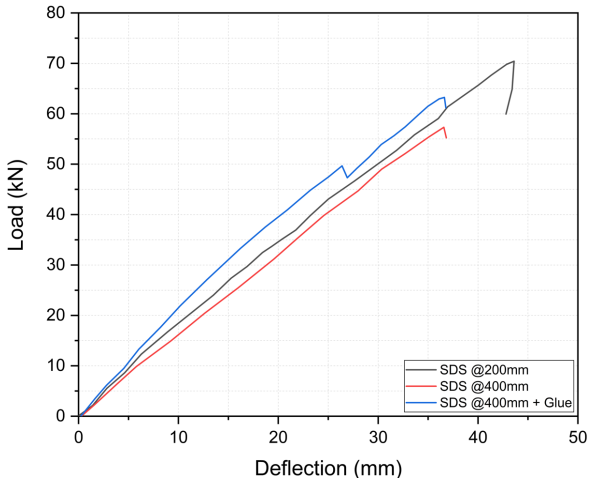

Fig. 9. Load deflection curves of the full scale specimens with self-drilling screws (SDS)

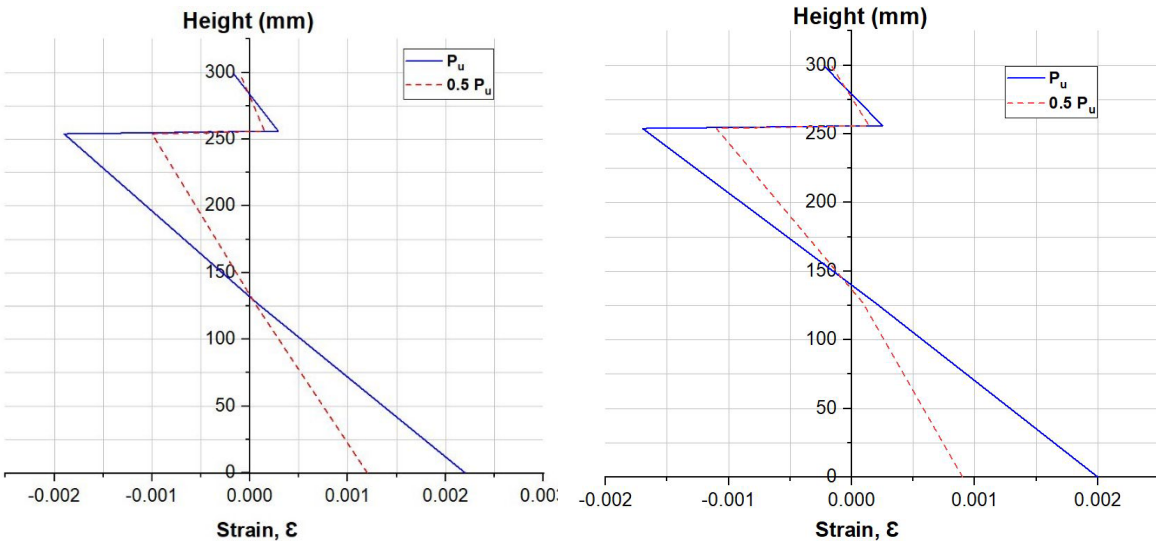

(a) (b)

Fig. 10. Strain distribution at mid-span section of specimens: (a) SP-3 (SDS @200mm) ; (b) SP-4 (SDS @400+Glue)

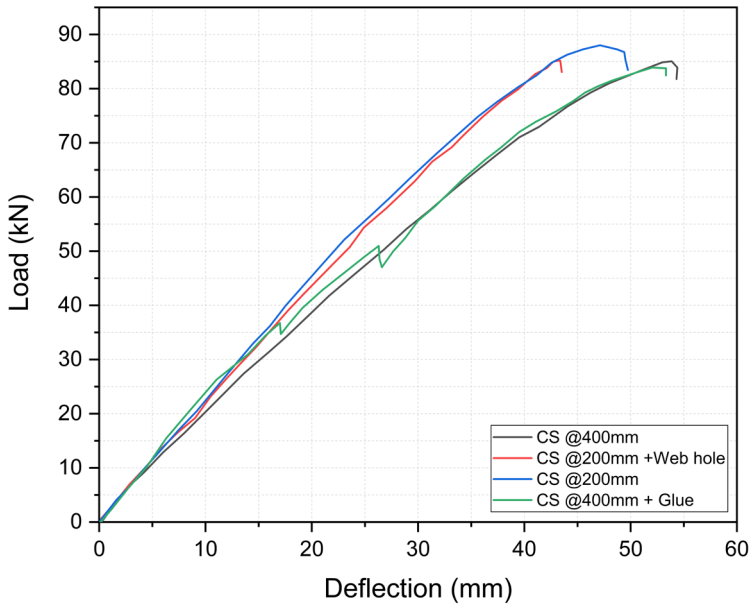

Fig. 11. Load deflection curves of the full scale specimens with M12 coach screws (CS)

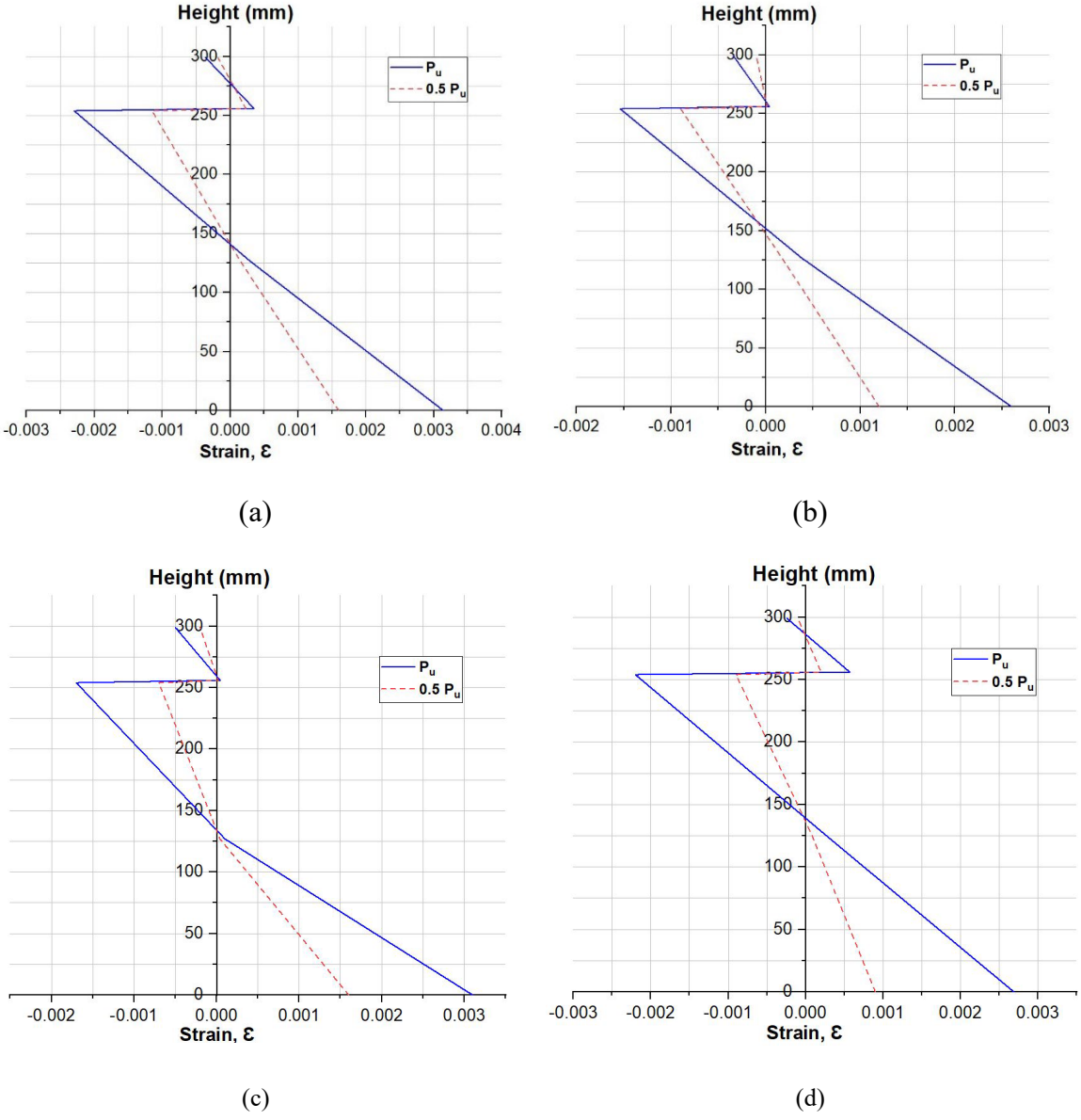

Fig. 12. Strain distribution at midspan section of specimens: (a) SP-5 (CS @400mm) ; (b) SP-6(CS @200); (c) SP-13 (CS @200+webhole); (d) SP-14 (CS @400+Glue)

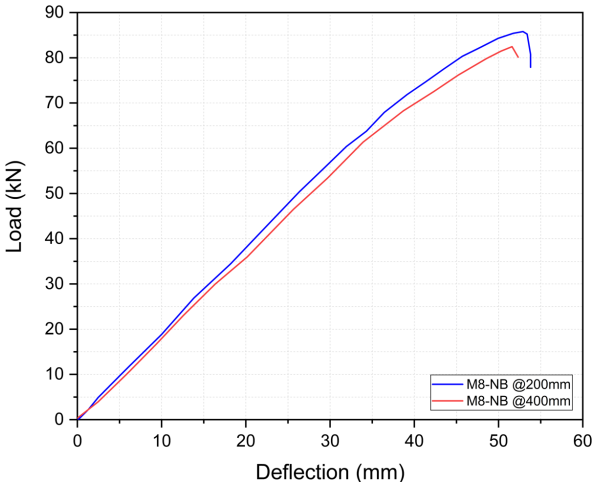

Fig. 13. Load deflection curves of the full scale specimens with M8 nuts and bolts

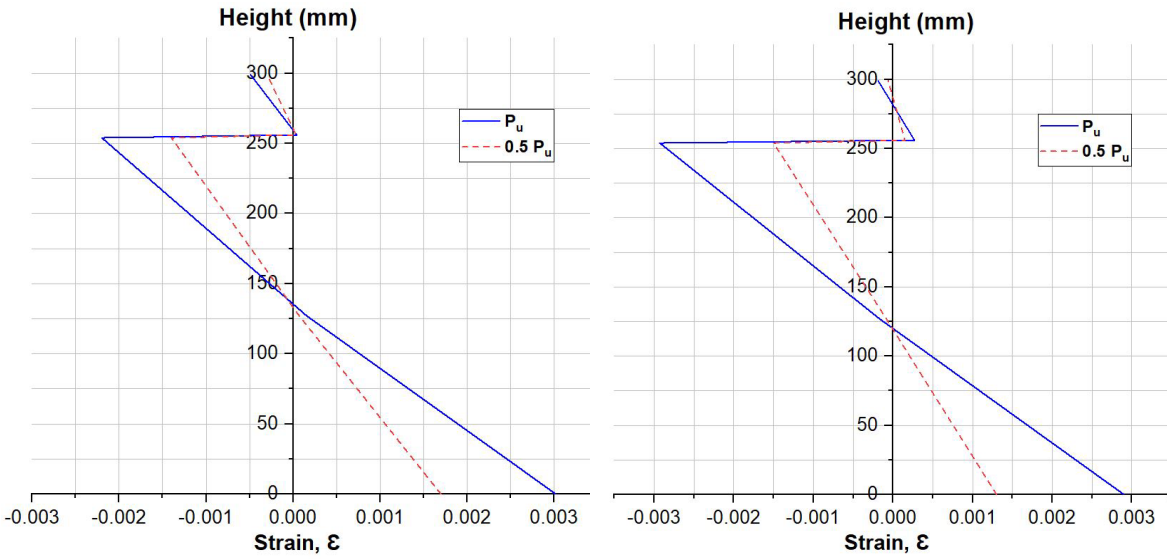

(a) (b)

Fig. 14. Strain distribution at mid-span section of specimens: (a) SP-10 (M8-NB @200mm) ; (b) SP-11 (M8-NB @400)

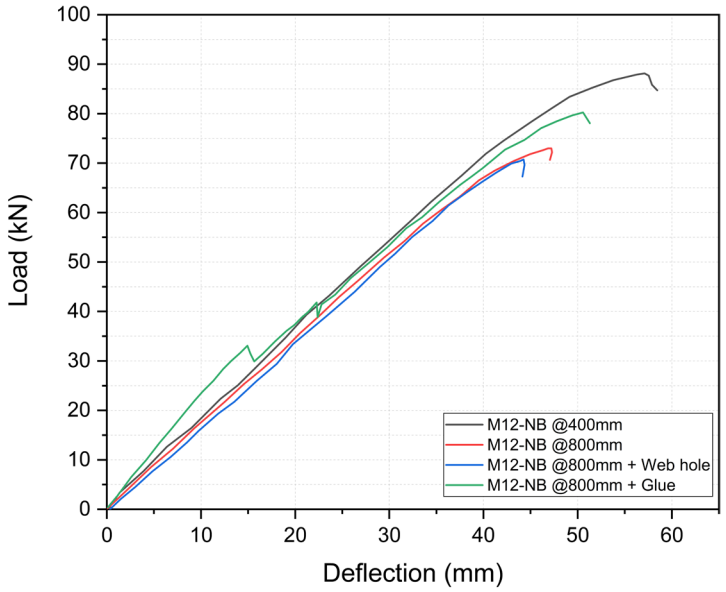

Fig. 15. Load deflection curves of the full scale specimens with M12 nuts and bolts

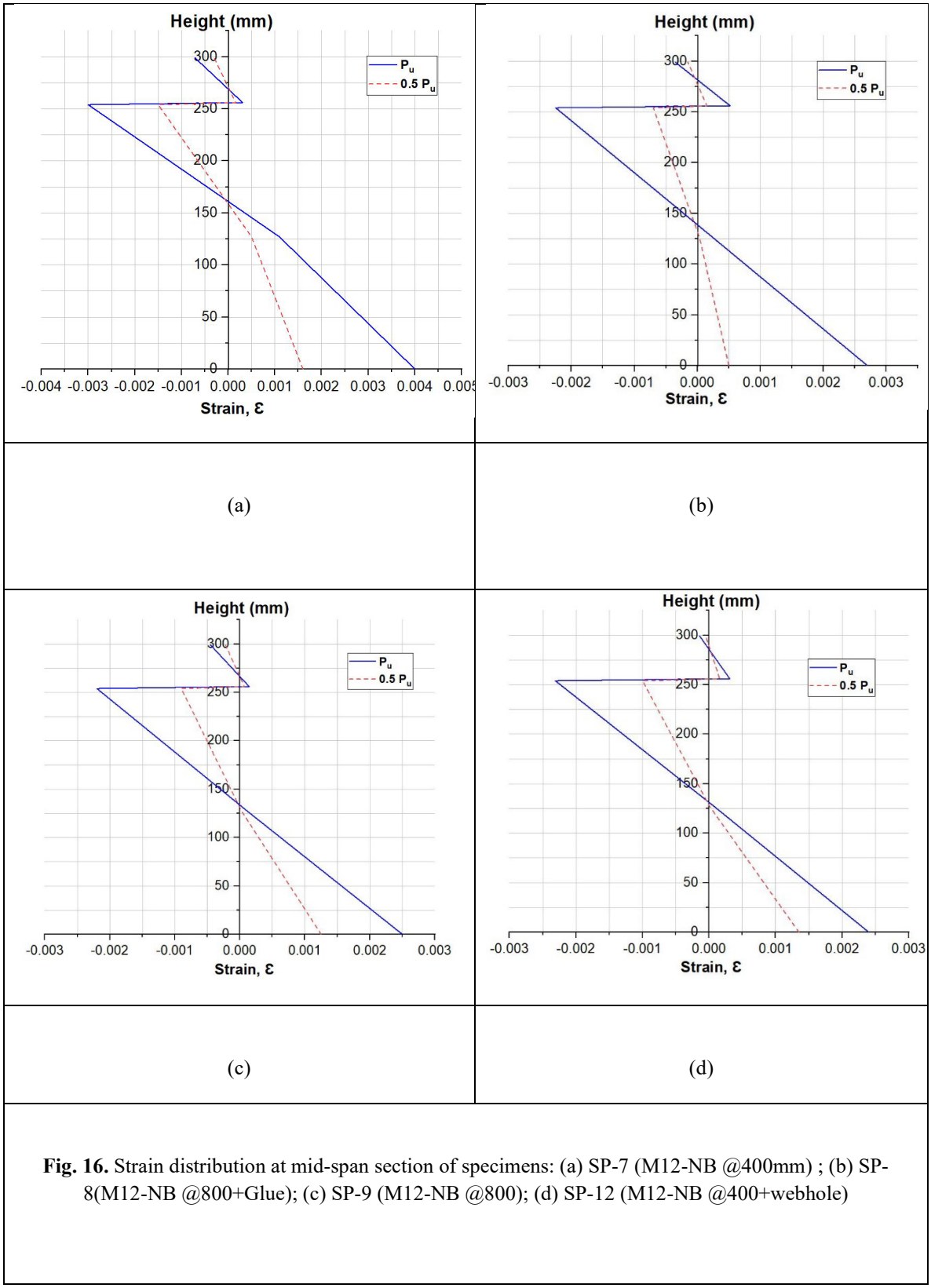

Fig. 16. Strain distribution at mid-span section of specimens: (a) SP-7 (M12-NB @400mm) ; (b) SP-8(M12-NB @800+Glue); (c) SP-9 (M12-NB @800); (d) SP-12 (M12-NB @400+webhole)

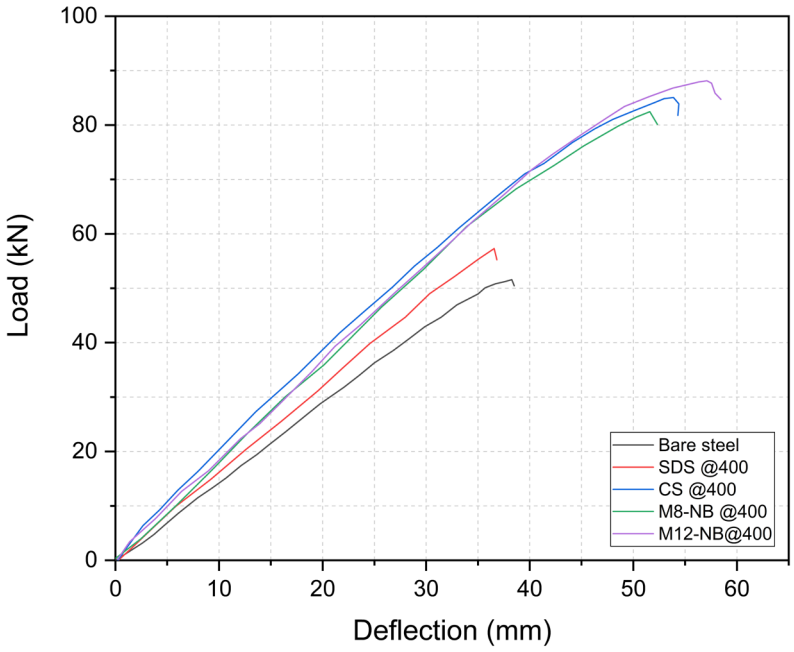

Fig. 17. Load deflection curves comparison of bare CFS with composite beams

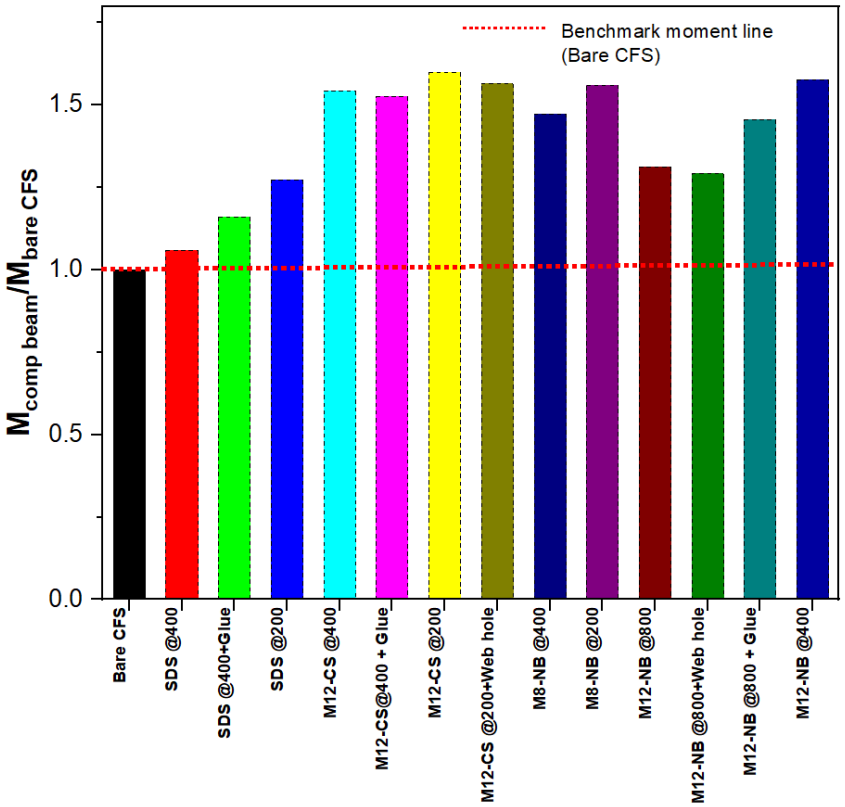

Fig. 18. Enhancement in moment capacity of the composite systems in comparison with bare CFS system

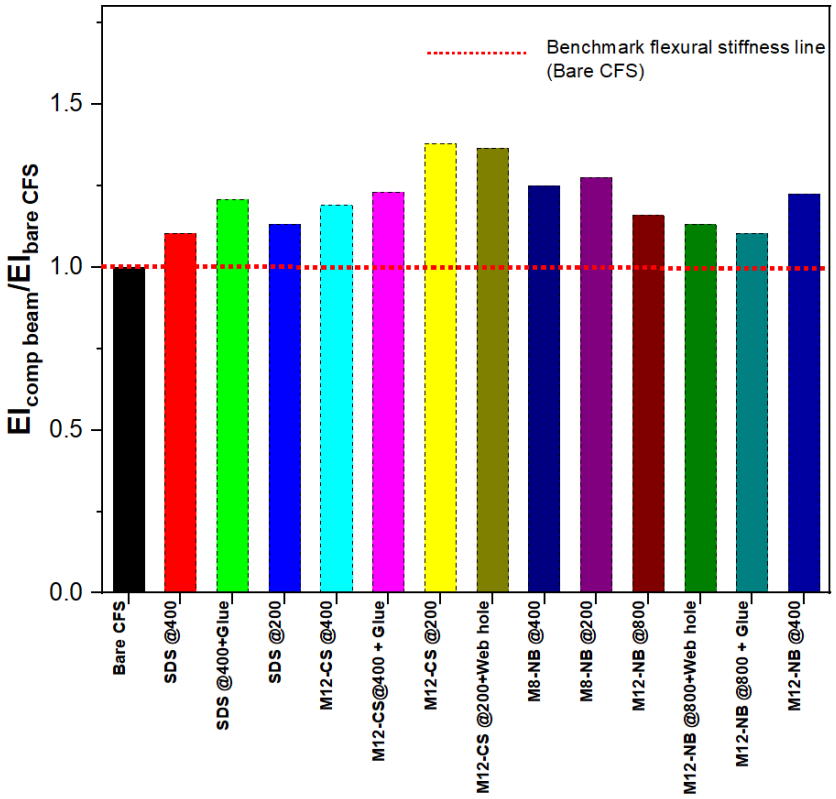

Fig. 19. Enhancement in flexural stiffness of the composite systems in comparison with bare CFS system

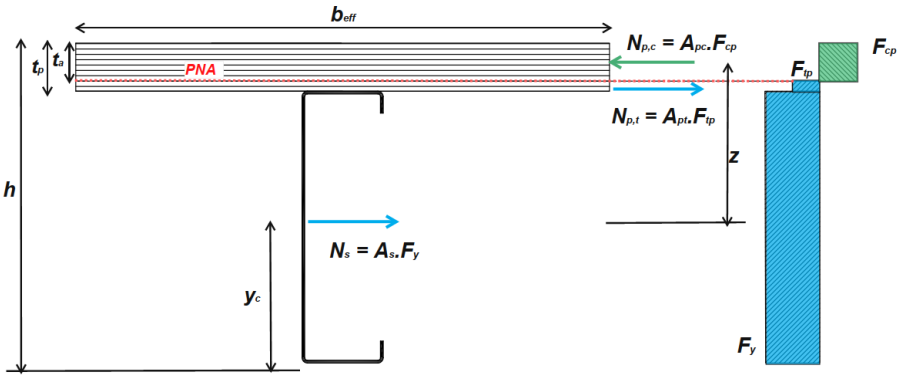
b_{eff}
t_p
t_a
PNA
h
y_c
$N_s = A_s.F_y$
$N_{p,c} = A_{pc}.F_{cp}$
$N_{p,t} = A_{pt}.F_{tp}$
z
F_{cp}
F_{tp}
F_y

Fig. 20. Distribution of plastic stress with the neutral axis in the floorboard sheathing

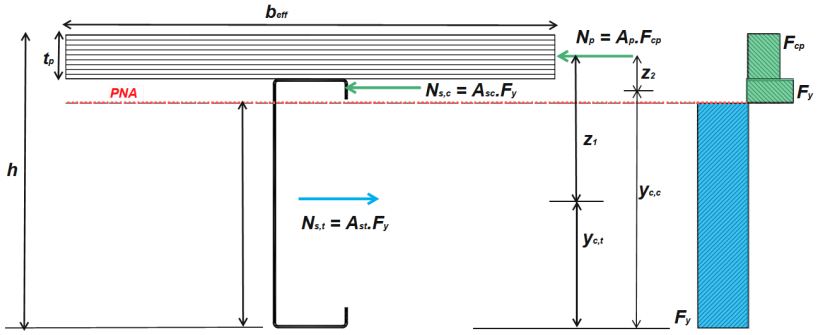

Fig. 21. Distribution of plastic stress with the neutral axis in the CFS joist

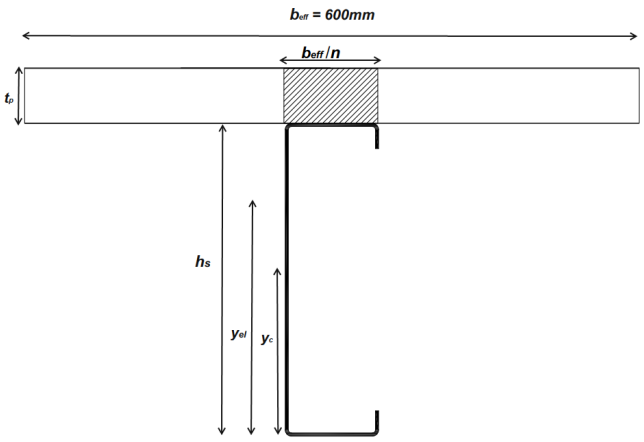

Fig. 22. Transformed section for the determination of stiffness of the composite system

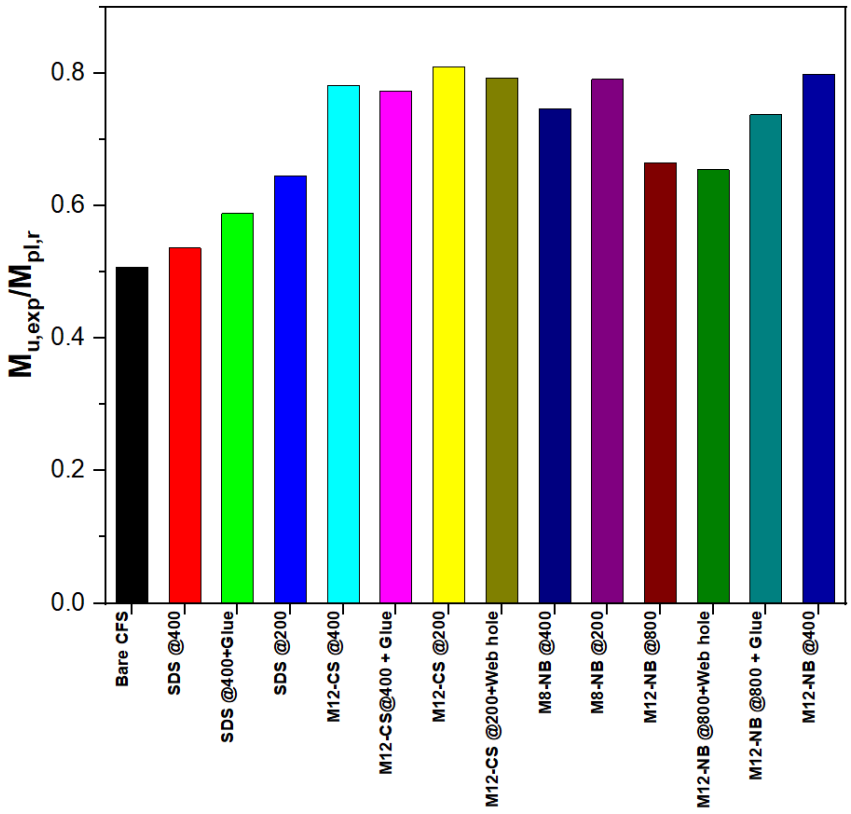

Fig. 23. Moment capacity of the composite systems relative to the corresponding theoretically fully composite system

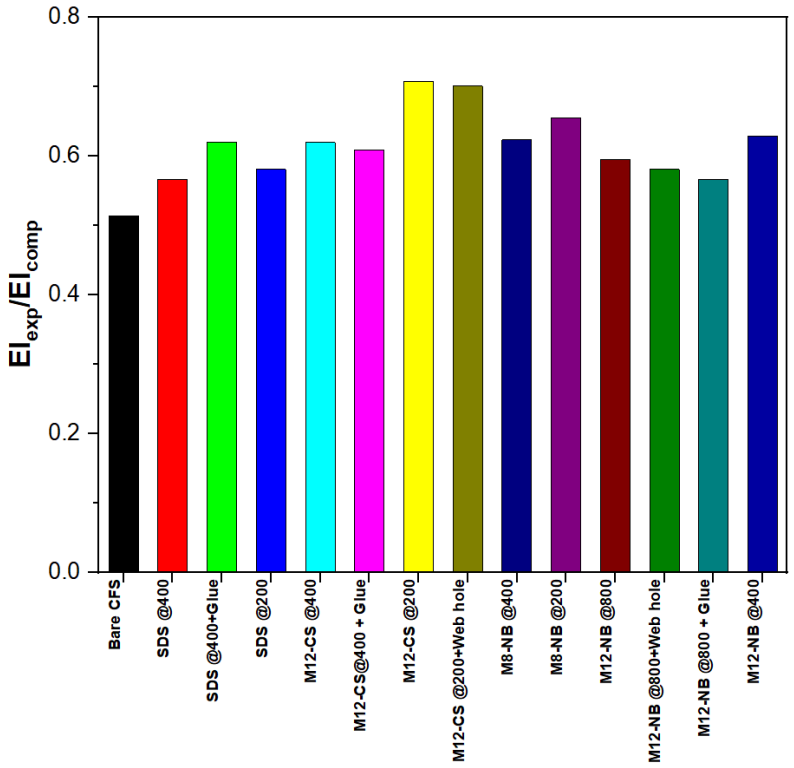

Fig. 24. Flexural stiffness of the composite systems relative to the corresponding theoretically fully composite system

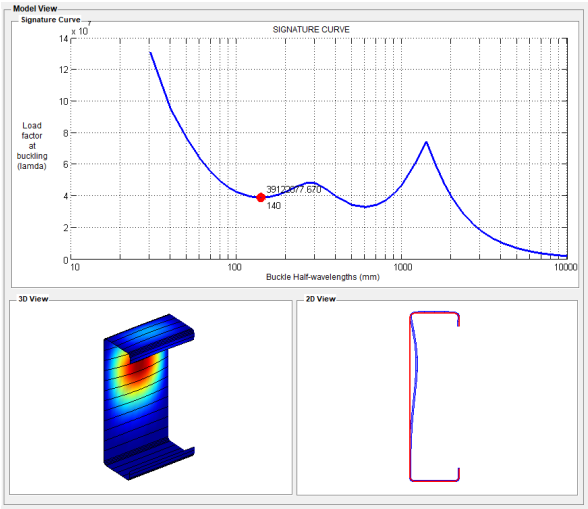

Fig. 25. Signature curve obtained from THIN WALL-2 for examined cold-formed steel C-section showing local buckling mode and half-wavelength

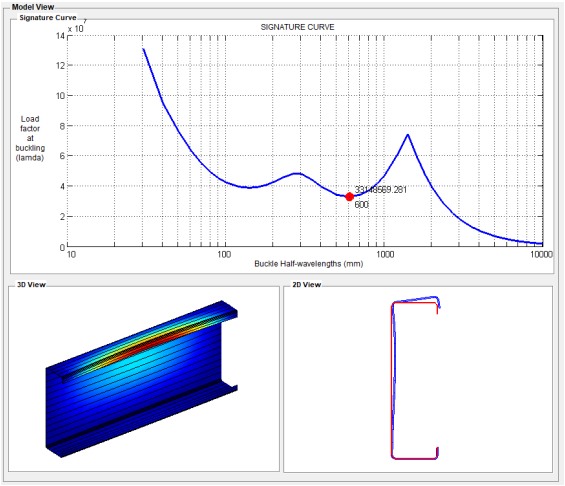

Fig. 26. Signature curve obtained from THIN WALL-2 for examined cold-formed steel C-section showing distortional buckling mode and half-wavelength

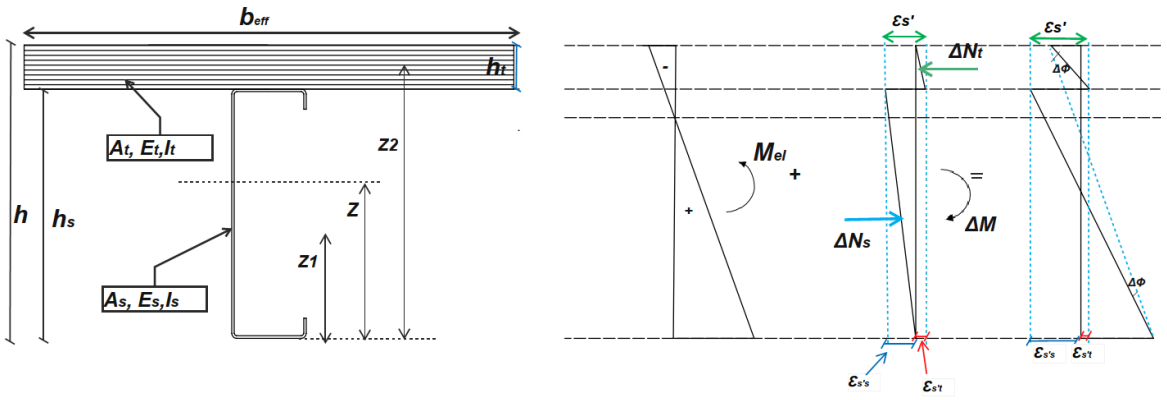

Fig. 27. Strain distribution in CFST beams under elastic bending

Table 1. Summary of push-out specimen details

Specimen	Web hole in joist	Type of shear connection	Spacing of shear connection	Structural adhesive at the beam-board interface
SP-1[a]	No	NA	NA	NA
SP-2	No	Self-drilling screw	400	No
SP-3	No	Self-drilling screw	200	No
SP-4	No	Self-drilling screw	400	Yes
SP-5	No	M 12 Coach screw	400	No
SP-6	No	M 12 Coach screw	200	No
SP-7	No	M12 nut and Bolt	400	No
SP-8	No	M12 nut and Bolt	800	No
SP-9	No	M12 nut and Bolt	800	Yes
SP-10	No	M8 nut and Bolt	200	No
SP-11	No	M8 nut and Bolt	400	No
SP-12	Yes	M12 nut and Bolt	800	No
SP-13	Yes	M 12 Coach screw	200	No
SP-14	No	M12 Coach screw	400	Yes

Table 2. Mechanical and geometrical properties of CFS beam

Thickness, t (mm)	Height (mm)	Flange width, b_f (mm)	Elastic modulus (MPa)	Yield strength (MPa)	Tensile strength (MPa)
2.4	254	76	207000	504	567

Table 3. Average measured mechanical properties of structural plywood (in MPa)

Bending parallel to grain ($f_{b,0}$)	Bending perpendicular to grain ($f_{b,90}$)	Tension parallel to grain ($f_{t,0}$)	Tension perpendicular to grain ($f_{t,90}$)	Compression parallel to grain ($f_{c,0}$)	Compression perpendicular to grain ($f_{c,90}$)	Modulus of Elasticity (E)
40	45.5	22	17	31.5	28	10000

Table 4. Key results of four-point bending tests of composite beam with self-drilling screws as shear connector

Specimen	M_u (kN.m)	EI ($N.m^2$)	δ_u (mm)	S_u (mm)
SDS at 200	52.5	2.65×10^6	43.6	2.6
SDS at 400	42.9	2.5×10^6	36.5	2.4
SDS at 400+glue	47	2.83×10^6	36.6	1.9
CS at 200	66	3.23×10^6	47.11	2.05
CS at 400	63.6	2.78×10^6	53.86	3.6
CS at 400+glue	62.9	2.83×10^6	52	2.2
CS at 200 + web holes in CFS joist	64.5	3.2×10^6	44	1.99
M8-NB at 200	64.35	2.99×10^6	53	3.2
M8-NB at 400	60.75	2.82×10^6	52.2	3.9
M12-NB at 400	66.05	2.87×10^6	57.1	4
M12-NB at 800	54.1	2.62×10^6	46.8	4.79
M12-NB at 800 + web hole in CFS joist	53.25	2.65×10^6	44.2	4.35
M12-NB at 800+Glue	60	2.7×10^6	50.5	4.15

Table 5. Four-point bending test results, elastic and plastic bending capacities of CFS C-section used in the study

P_u (kN)	M_t (kN.m)	F_{ol} (mPa)	F_{od} (mPa)	Z (mm^3)	S_x (mm^3)	M_{ol} (kN.m)	M_{od} (kN.m)	M_y (kN.m)	M_p (kN.m)
52.5	39.37	509	430	75651	83530	39.1	32.5	38.12	43

Table 6. Comparison of effective bending stiffness from experiment and Gamma method and composite efficiency for CFST beams

Specimen	EI_{exp} ($N.m^2$)	$EI_{partial,\ \gamma\text{-method}}$ ($N.m^2$)	$EI_{partial,\ \gamma\text{-method}}/EI_{exp}$	Composite efficiency (%)
SP-2	2.65×10^6	2.5×10^6	0.96	17.5
SP-3	2.7×10^6	2.82×10^6	1.06	30.4
SP-4	2.83×10^6	2.8×10^6	1	30.5
SP-5	2.8×10^6	2.96×10^6	1.05	36
SP-6	3.2×10^6	3.44×10^6	1.06	55
SP-7	2.9×10^6	2.84×10^6	0.99	31
SP-8	2.6×10^6	2.51×10^6	0.97	18
SP-9	2.7×10^6	2.7×10^6	0.98	24.5
SP-10	3×10^6	2.9×10^6	0.97	36
SP-11	2.8×10^6	2.6×10^6	0.9	22
SP-12	2.7×10^6	2.9×10^6	1.12	36
SP-13	3.2×10^6	3.4×10^6	1.07	55
SP-14	2.8×10^6	3×10^6	1.08	38

Table 7. Comparison of theoretical elastic bending moment values with test values

Specimen	$M_{u,exp}$ (kN.m)	M_{el} (kN.m)	ΔM (kN.m)	M (kN.m)	$M_{u,exp}/M$	δ_{exp} (mm)	$\delta_{analytical}$ (mm)	Relative Error (%)
SP-2	43.65	59.8	14.3	45.5	0.96	36.5	37.7	-3.2
SP-3	51.5	59.8	10	49.8	1.05	43.6	40.11	8.7
SP-4	47.85	59.8	9.6	50.2	0.95	36.6	36.55	0.13
SP-5	63.6	59.8	10	49.8	1.28	53.86	46.33	16.2
SP-6	65.89	59.8	7.24	52.56	1.25	47.11	41.35	13.9
SP-7	65	59.8	8.5	51.3	1.27	57.1	49.37	15.65
SP-8	54.1	59.8	14.2	45.6	1.19	46.8	46.53	0.58
SP-9	60	59.8	10.25	49.55	1.21	50.5	48.5	4
SP-10	64.35	59.8	8.5	51.3	1.25	53	47.8	10.8
SP-11	60.75	59.8	10.65	49.15	1.24	52.2	51.4	1.56
SP-12	53.25	59.8	10	49.8	1.07	44.2	38.79	13.9
SP-13	64.5	59.8	5.4	54.4	1.19	44	40.48	8.7
SP-14	62.9	59.8	9	50.8	1.24	52	45.2	15